Spectrum of Light Quasi-Elastically Scattered from Solutions of Semiflexible Filaments in the Dilute and Semidilute Regimes†

Tadakazu Maeda and Satoru Fujime*

Mitsubishi-Kasei Institute of Life Sciences, Machida, Tokyo 194, Japan.
Received February 7, 1984

ABSTRACT: A theoretical model is considered for the effect of anisotropic translational diffusion and filament flexibility on the polarized field correlation function $G^1(\tau)$ of light quasi-elastically scattered from solutions of very long, semiflexible filaments. Our previous results on flexing motions of a semiflexible filament[19] and on the Green function to the coupled translational/rotational diffusion equation for a long rod[16] have been combined to obtain a general expression for $G^1(\tau)$. The expression contains a fourfold integration over orientation at times t and t' ($\tau \equiv |t - t'|$) of the long axis of the rod relative to the scattering vector $\vec{K}$ and over coordinates s and s' on the rod. Numerical studies showed that the fourfold integration can be reduced to a threefold integration with high accuracy. For an approximate method, even twofold integration can be used to simulate $G^1(\tau)$. Numerical results will be presented to visualize our model. In the framework of the Doi–Edwards model,[18] our theory can be directly extended to the case of a semidilute solution of a semiflexible filament. Our model was applied to analyze experimental data available in the literature on fd virus (length L = 895 nm, diameter d = 9 nm) both in dilute and semidilute solution. We could estimate the flexibility parameter of fd virus from experimental data for dilute solution. Our analysis of experimental data for semidilute solutions suggested that the sideways translational diffusion constant is not small compared with that in dilute solution when KL is large, where K is the length of $\vec{K}$.

1. Introduction

Quasi-elastic scattering of laser light has been extensively applied to dynamic studies of macromolecules in solution. We have been interested in the dynamics of very long and semiflexible (or slightly bendable) filaments in solution. Such filaments include muscle F-actin and its complexes with other muscle proteins,[1-7] bacterial flagellum,[8] various kinds of rodlike viruses,[9,10] microtuble,[11] and muscle thin[10] and thick[11] filaments. For example, the thin filament of skeletal muscle is 1 μm in length (L) and 5–8 nm in diameter (d).

To interpret experimental spectra (time correlation functions $G^1(\tau)$ or power spectra of light scattered) from solutions of such long and semiflexible filaments, theoretical models for rigid rods undergoing translational and rotational Brownian motions are usually applied as a first-order approximation. Because a long rod undergoes anisotropic translation, a coupling between translational and rotational modes of diffusive motions is expected. This effect has been studied with special reference to tobacco mosaic virus.[13,14] In this case, however, the experimental results excluded the coupling effect,[14] and no further study has been made of this effect either theoretically or experimentally. But, if one wants to study very long rods, one has to take account for the coupling effect. Recently, this coupling effect has been again discussed[15-17] and recognized to be very important at any KL value except very small ones, where K is the length of the momentum transfer vector. Following the notation in ref 16, the first cumulant $\bar{\Gamma}$ of $G^1(\tau)$ is given by

$$\bar{\Gamma}/K^2 = [D - \tfrac{1}{3}(D_3 - D_1)] + (L^2/12)\Theta f_1(k) + (D_3 - D_1)f_2(k)$$

where D, D_3, D_1, and Θ are, respectively, the overall, lengthways, sideways translational, and the rotational diffusion constants, and $f_1(k)$ and $f_2(k)$ are functions depending only on $k = KL/2$.

In addition to the coupling effect, one has to take account of the effect of entanglements of long rods in semidilute solution. Let c be the number of rods in unit volume. Then, one has to distinguish the two cases $cL^3 \ll 1$ (dilute regime) and $L/d \gg cL^3 \gg 1$ (semidilute regime). In the case of muscle thin filaments; for example, 1 mg/mL protein corresponds to $cL^3 = 40$. Doi and Edwards considered the light-scattering spectra from semidilute solutions of rigid rods.[18] In the framework of their model, we have considered the light-scattering spectra from solutions of very long rods.[16]

Even if rods seem (or are believed) to be rigid, they might be semiflexible when they are very long. On electron micrographs of all the above-mentioned filaments, one clearly observes slightly curved images. Thus one has to take account of the effect of filament flexibility on the spectra. Experimentally speaking, if the observed $\bar{\Gamma}$ values exceed the theoretical values given by the above equation, one has to consider a possible contribution from filament flexibility. We have published a paper on the effect of filament flexibility on light-scattering spectra,[19] where neither the coupling effect nor the entanglement was considered.

In this paper, we first review briefly our model of the micro-Brownian motion of a semiflexible filament[19] and the Green function to the coupled translational/rotational diffusion equation.[16] Then the light-scattering problems of semiflexible filaments will be considered in the following order: semiflexible filaments in dilute solution where the coupling and the flexibility effects will be discussed; semiflexible filaments in semidilute solution where the coupling, the entanglement, and the flexibility effects will be discussed; then some examples of computer simulation of correlation functions will be presented in order to visualize the model; finally, an application of our model will be made to experimental data, available in the literature, for fd virus (L = 895 nm and d = 9 nm) in dilute and semidilute solutions. Because the main aim of this paper is to show gross features characteristic of polarized light-scattering spectra for solutions of very long and semiflexible filaments in the dilute and semidilute regimes, a very simple model will be adopted and no sophisticated interaction will be considered. An outline of this study has been published.[20]

2. Model

We consider a spectrum of light quasi-elastically scattered from solutions of long, thin and semiflexible filaments. For this purpose, let us define the conformation

† Part of this study was presented at the Cambridge Conference on "Biomedical Application of Laser Light Scattering", Cambridge, Sept 1981.

0024-9297/84/2217-2381$01.50/0 © 1984 American Chemical Society

of a filament by a space curve $\vec{r}(s,t)$, where s is the coordinate of the line element ds (or a segment) measured along the chain having the contour length L ($L/2 \geq s \geq -L/2$) and t is time. The elastic potential energy V for a slightly bendable filament will be given by

$$V = \frac{\epsilon}{2}\int_{-L/2}^{L/2}(\partial^2\vec{r}(s,t)/\partial s^2)^2\, ds \tag{1}$$

where ϵ is a suitably defined flexural rigidity. From eq 1, the Langevin equation for a semiflexible filament is derived as

$$\rho(\partial^2\vec{r}/\partial t^2) + \zeta(\partial\vec{r}/\partial t) + \epsilon(\partial^4\vec{r}/\partial s^4) = \vec{A}(s,t) \tag{2}$$

where ρ is the linear mass density of the filament, ζ is the friction constant per unit length of the filament, and $\vec{A}$ is the fluctuating Brownian force acting on the filament. By mode expansion

$$\vec{r}(s,t) = \sum_m \vec{q}(m,t)Q(m,s) \tag{3a}$$

$$\vec{A}(s,t) = \sum_m \vec{B}(m,t)Q(m,s) \tag{3b}$$

eq 2 is written as

$$\rho\vec{q}'' + \zeta\vec{q}' + \lambda_m\vec{q}(m,t) = \vec{B}(m,t) \tag{4a}$$

$$\epsilon Q^{IV}(m,s) = \lambda_m Q(m,s) \tag{4b}$$

Equation 4b with free-end boundary conditions, $Q^{III}(m,s) = Q^{II}(m,s) = 0$ at $s = \pm L/2$, gives eigenvalues λ_m:

$$\lambda_0 = \lambda_1 = 0 \tag{5a}$$

and

$$\lambda_m = \epsilon\pi^4(m - \tfrac{1}{2})^4/L^4 \qquad (m \geq 2) \tag{5b}$$

Eigenfunctions $Q(m,s)$ have the forms of

$$Q(0,s) = (1/L)^{1/2}, \qquad Q(1,s) = (12/L^3)^{1/2}s \tag{6a}$$

$$Q(m,s) = \left(\frac{1}{L}\right)^{1/2}\left[\frac{\sin(\beta_m s)}{\sin(\beta_m L/2)} + \frac{\sinh(\beta_m s)}{\sinh(\beta_m L/2)}\right] \qquad \text{(odd } m\text{)} \tag{6b}$$

$$Q(m,s) = \left(\frac{1}{L}\right)^{1/2}\left[\frac{\cos(\beta_m s)}{\cos(\beta_m L/2)} + \frac{\cosh(\beta_m s)}{\cosh(\beta_m L/2)}\right] \qquad \text{(even } m\text{)} \tag{6c}$$

where $\beta_m = (\lambda_m/\epsilon)^{1/4}$. From eq 1 and 3a, we have

$$V = (1/2)\sum_m \lambda_m\vec{q}(m,t)^2 \tag{7}$$

This relation determines the expectation values $\langle\vec{q}(m,t)^2\rangle$ for $m \geq 2$ (for which $\lambda_m \neq 0$). However, it does not determine the expectation values for the $m = 0$ and 1 modes in the same way. To overcome this difficulty, we need another approach. From eq 6a and 3a, we have relations for transformation from *molecule-fixed coordinates*, $\vec{q}(0,t)$ and $\vec{q}(1,t)$, to *laboratory-fixed coordinates*, $\vec{R}(t)$ and $\vec{t}(t)$:

$$\vec{q}(0,t) = (1/L)^{1/2}\int\vec{r}(s,t)\, ds = L^{1/2}\vec{R}(t) \tag{8a}$$

$$\vec{q}(1,t) = (12/L^3)^{1/2}\int\vec{r}(s,t)s\, ds = (L^3/12)^{1/2}\vec{t}(t) \tag{8b}$$

where $\vec{R}(t)$ is the position vector of the center-of-mass of the filament and $\vec{t}(t)$ is the unit vector parallel to the filament in its straight form. Then eq 3a is written as

$$\vec{r}(s,t) = \vec{R}(t) + s\vec{t}(t) + \sum{}''\vec{q}(m,t)Q(m,s) \tag{9}$$

Each $\vec{q}(m,t)$ in eq 9 has mutually perpendicular components $[q_1(m,t), q_2(m,t), q_3(m,t)]$. Setting $q_3(m,t)$ parallel to $\vec{t}(t)$, the orientation relation between molecule-fixed coordinates $\vec{q}(m,t)$ and the laboratory-fixed coordinate $\vec{t}(t)$ can be defined. Because $q_1(m,t)Q(m,s)$ and $q_2(m,t)Q(m,s)$ represent the lateral (bending) motions of the filament and $q_3(m,t)Q(m,s)$ represents the longitudinal (stretch/contraction) motion of the filament, we have to put $q_3(m,t) = 0$ for all $m \geq 2$. Then eq 9 has a very simple geometrical meaning as shown in Figure 1. Equation 3b is also written as

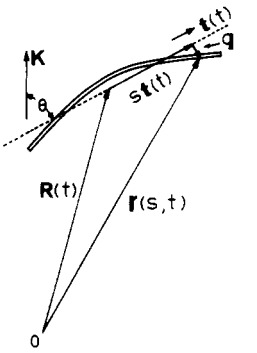

Figure 1. Geometrical relationship among various vectors defining the position vector $\vec{r}(s,t)$ of the line element ds of a semiflexible filament. $\vec{K}$ is the scattering vector, $\vec{t}(t)$ is the unit vector indicating the instantaneous orientation of the "mean" axis, $\vec{q}$ is the amplitude of the bending motion, $\vec{R}(t)$ is the position vector of the center-of-mass, and θ is the instantaneous angle between $\vec{K}$ and $\vec{t}$.

$$\vec{A}(s,t) = \vec{F}(t)/L + s\vec{T}(t)(12/L^3) + \sum{}''\vec{B}(m,t)Q(m,s) \tag{10}$$

where $\vec{F}(t) = \int\vec{A}(s,t)\, ds$ is the random force acting on $\vec{R}(t)$, and $\vec{T}(t) = \int\vec{A}(s,t)s\, ds$ is the random torque acting on $\vec{t}(t)$. By using eq 9 and 10, we write eq 4 for $m = 0$ and 1 as

$$M\vec{R}''(t) + \Xi_{tr}\vec{R}'(t) = \vec{F}(t) \tag{11a}$$

$$I\vec{t}''(t) + \Xi_{rot}\vec{t}'(t) = \vec{T}(t) \tag{11b}$$

where $M = \rho L$, $\Xi_{tr} = \zeta L$, $I = \rho L^3/12$ (the moment of inertia of the rod around its minor axis), and $\Xi_{rot} = \zeta L^3/12$. Equation 11a represents the translational Brownian motion. Equation 11b represents the rotational Brownian motion because the time derivative of the unit vector $\vec{t}(t)$ can be regarded as the angular velocity of the rod rotating around its minor axis. A long rod undergoes anisotropic translational diffusion as well as rotational diffusion. Diffusion constants are given by

$$D_1 = D_2 = k_BT/\Xi_{tr} = k_BT/(\zeta L) \qquad \text{(sideways translation)} \tag{12a}$$

$$D_3 = k_BT/(\zeta_\parallel L) \qquad \text{(lengthways translation)} \tag{12b}$$

$$\Theta = k_BT/\Xi_{rot} = 12D_1/L^2 \qquad \text{(end-over-end rotation)} \tag{12c}$$

where $\zeta_\parallel = \zeta/2$ in the long-rod limit. Diffusion problems will be discussed later.

For $m \geq 2$, eq 4a and 7 give, under the usual approximations

$$\langle\vec{q}(m,t)\vec{q}(m',t')\rangle = \langle\vec{q}(m,t)^2\rangle\exp(-\tau/\tau_m)\delta_{mm'} \tag{13}$$

$$\langle q_m^2\rangle = \langle\vec{q}(m,t)^2\rangle = \langle q_1(m,t)^2\rangle + \langle q_2(m,t)^2\rangle = 2k_BT/\lambda_m \tag{14}$$

$$\tau_m = \zeta/\lambda_m \tag{15}$$

where $\tau = |t - t'|$ and $\delta_{mm'}$ is the *Kronecker* delta.

The unnormalized field correlation function $G^1(\tau)$ of scattered light is given by

$$G^1(\tau) = (1/L^2)\int\int_{-L/2}^{L/2} J(s,s',\tau)\, ds\, ds' \quad (16)$$

$$J(s,s',\tau) = \langle \exp[i\vec{K}\cdot\{\vec{r}(s,t) - \vec{r}(s',t')\}]\rangle \quad (17)$$

where $\vec{K}$ is the momentum transfer vector.

For the case of a rigid rod (i.e., $\vec{q}(m,t) = 0$ in eq 9), we have shown that

$$J(s,s',\tau) = G_D(\tau)\left[\frac{1}{2}\int\int_{-1}^{1} e^{iK(s\xi - s'\xi')} g_K(\xi,\xi';\tau)\, d\xi\, d\xi'\right] \quad (18)$$

$$G_D(\tau) = \exp[-\{D - \tfrac{1}{3}(D_3 - D_1)\}K^2\tau] \equiv \exp(-D_1K^2\tau) \quad (19)$$

where $\xi = \xi(t) = \cos\theta(t)$ (see Figure 1), $\xi' = \xi(t')$, and $g_K(\xi,\xi';\tau)$ is the Green function which satisfies the translational/rotational diffusion equation for a rod:

$$[\partial/\partial\tau - \Theta(\nabla_\xi^2 - \mu^2\xi^2)]g_K(\xi,\xi';\tau) = \delta(\xi - \xi')\delta(\tau) \quad (20)$$

$$\mu^2 = (D_3 - D_1)K^2/\Theta \quad (21)$$

The parameter μ^2 is the coupling constant between translational and rotational modes of diffusive motion. When we put

$$g_K(\xi,\xi';\tau) = \sum_n A_n(K,\xi',\tau)P_n(\xi) \quad (22)$$

where $P_n(\xi)$ is the Legendre polynomial, we have from eq 20 (see ref 16)

$$\partial A_n/\partial(\Theta\tau) = -[n(n+1) + \mu^2L_0(n)]A_n - \mu^2L_1(n)A_{n-2} - \mu^2L_2(n)A_{n+2} \quad (23)$$

with the initial condition

$$A_n(K,\xi',0) = \frac{2n+1}{2}P_n(\xi') \quad (24)$$

Since there is no coupling between A_n and A_{n+1} in eq 23, let us define, for an appropriate even integer N, vectors $\mathbf{A}^e = (A_0, A_2, ..., A_N)^T$ and $\mathbf{A}^o = (A_1, A_3, ..., A_{N+1})^T$ (T designates transposition) and matrices $\mathbf{M}^e$ and $\mathbf{M}^o$ consiting of coefficients in eq 23 (see ref 16). Then eq 23 is written in a matrix form as

$$\partial/\partial(\Theta\tau)\begin{bmatrix}\mathbf{A}^e\\ \\ \mathbf{A}^o\end{bmatrix} = -\begin{bmatrix}\mathbf{M}^e & \mathbf{0}\\ \\ \mathbf{0} & \mathbf{M}^o\end{bmatrix}\begin{bmatrix}\mathbf{A}^e\\ \\ \mathbf{A}^o\end{bmatrix} \quad (25)$$

Let us define $\mathbf{U}$ and $\mathbf{V}$, which satisfy, respectively,

$$\mathbf{U}^{-1}\mathbf{M}^e\mathbf{U} = \mathbf{\Lambda}^e = \{\lambda_p{}^e\delta_{pp'}\} \quad (26a)$$

and

$$\mathbf{V}^{-1}\mathbf{M}^o\mathbf{V} = \mathbf{\Lambda}^o = \{\lambda_p{}^o\delta_{pp'}\} \quad (26b)$$

Then we have[21]

$$A_n = \sum_{l\ \text{even}} [\mathbf{U}\exp(-\mathbf{\Lambda}^e\Theta\tau)\mathbf{U}^{-1}]_{n,l}A_l(0) \qquad (\text{for even } n) \quad (27a)$$

$$A_n = \sum_{l\ \text{odd}} [\mathbf{V}\exp(-\mathbf{\Lambda}^o\Theta\tau)\mathbf{V}^{-1}]_{n,l}A_l(0) \qquad (\text{for odd } n) \quad (27b)$$

From eq 22, 24, and 27, we have

$$g_K(\xi,\xi';\tau) = g_K{}^e(\xi,\xi';\tau) + g_K{}^o(\xi,\xi';\tau) \quad (28a)$$

$$g_K{}^e(\xi,\xi';\tau) = \sum_{n\ \text{even}}\sum_{l\ \text{even}} \frac{2l+1}{2}[\mathbf{U}\exp(-\mathbf{\Lambda}^e\Theta\tau)\mathbf{U}^{-1}]_{n,l}P_n(\xi)P_l(\xi') \quad (28b)$$

$$g_K{}^o(\xi,\xi';\tau) = \sum_{n\ \text{odd}}\sum_{l\ \text{odd}} \frac{2l+1}{2}[\mathbf{V}\exp(-\mathbf{\Lambda}^o\Theta\tau)\mathbf{V}^{-1}]_{n,l}P_n(\xi)P_l(\xi') \quad (28c)$$

For $g_K(\xi,\xi';\tau)$ in eq 18, we need only $g_K{}^e(\xi,\xi';\tau)$. However, when we extend eq 18 to the case of semiflexible filaments, we need both $g_K{}^e(\xi,\xi';\tau)$ and $g_K{}^o(\xi,\xi';\tau)$.

For large μ^2 values ($\mu^2 \geq 50$), we have another simple form of $g_K(\xi,\xi';\tau)$:

$$g_K{}^{\gg}(\xi,\xi';\tau) = \left[\frac{\mu}{2\pi\sinh(2\mu\Theta\tau)}\right]^{1/2} \times \exp\left[-\mu\frac{(\xi^2+\xi'^2)\cosh(2\mu\Theta\tau) - 2\xi\xi'}{2\sinh(2\mu\Theta\tau)}\right] \quad (29a)$$

$$= \left[\frac{\mu}{2\pi\sinh(2\mu\Theta\tau)}\right]^{1/2} \times \exp\left[-\frac{\mu}{4}(\xi-\xi')^2/\tanh(\mu\Theta\tau)\right] \times \exp\left[-\frac{\mu}{4}(\xi+\xi')^2\tanh(\mu\Theta\tau)\right] \quad (29b)$$

where the superscript $\gg$ attached to $g_K(\xi,\xi';\tau)$ means $\mu \gg 1$.

3. Semiflexible Filaments in Dilute Solution

The coupling-term $\mu^2\xi^2$ in eq 20 between translational and rotational diffusion comes from the fact that the translation of the center-of-mass of a rod in a given direction depends on the orientation of the rod because of $D_3 \neq D_1$. This is the first-order effect of the coupling. It is theoretically possible, for example, that the end-over-end rotation of the rod is differently influenced whether the rod undergoes sideways or lenghways translation.[22] This, however, is the second-order effect on diffusive motions. Likewise, bending motions of a slightly bendable filament will be independent, to the first-order approximation, of anisotropic translation as well as rotation of the rod.

The laboratory-fixed coordinates $[X,Y,Z]$ and the molecule-fixed coordinates (1,2,3) are related to each other by the Eulerian angles ψ, ϕ, and θ. Using these angles, we have $\vec{K} = [0,0,K] = (-K\cos\psi\sin\theta, K\sin\psi\sin\theta, K\cos\theta)$ and hence

$$\vec{K}\cdot\vec{q}(m,t) = -Kq_1(m,t)\cos\psi\sin\theta + Kq_2(m,t)\sin\psi\sin\theta \quad (30)$$

$$\langle[\vec{K}\cdot\vec{q}(m,t)][\vec{K}\cdot\vec{q}(m,t')]\rangle = (K^2/2)\langle q_m{}^2\rangle\exp(-\tau/\tau_m)\cos(\psi-\psi')\sin\theta\sin\theta' \quad (31)$$

Although not considered explicitly, the rotation around the dotted line in Figure 1 has no effect because of $\langle q_1(m,t)^2\rangle = \langle q_2(m,t)^2\rangle = (1/2)\langle q_m{}^2\rangle$; that is, we may put in effect $\cos(\psi-\psi') = 1$. Then we have

$$J(s,s',\tau) = G_D(\tau)\left[\frac{1}{2}\int\int_{-1}^{1} d\xi\, d\xi'\, g_K(\xi,\xi';\tau)\exp[iK(s\xi - s'\xi')]\prod_{m\geq 2}\exp[-\Phi(m,s,s',\xi,\xi',\tau)]\right] \quad (32)$$

$$\Phi(m,s,s',\xi,\xi',\tau) = (K^2/4)\langle q_m{}^2\rangle\{(1-\xi^2)Q(m,s)^2 + (1-\xi'^2)Q(m,s')^2 - 2[(1-\xi^2)(1-\xi'^2)]^{1/2}Q(m,s)Q(m,s')\exp(-\tau/\tau_m)\} \quad (33)$$

For the Green function in eq 32, we can use eq 28 or 29. Without numerical integration of eq 32 with eq 16, we cannot know the time behavior of $G^1(\tau)$. However, the first

cumulant $\bar{\Gamma}$ of $G^1(\tau)$ has a very simple form, especially at $KL \gg 1$.

Since $\langle q_m{}^2\rangle/\tau_m = 2k_BT/\zeta$, we have from eq 32

$$\bar{\Gamma} = -\frac{\partial}{\partial\tau}\ln G^1(\tau)|_{\tau=0} = [D - \tfrac{1}{3}(D_3 - D_1)]K^2 + \frac{1}{G^1(0)}\frac{1}{2L^2}\int\int ds\, ds' \left\{-\int\int\left[\Psi(s,s',\xi,\xi',\tau)\frac{\partial}{\partial\tau}g_K(\xi,\xi';\tau)\right]_{\tau=0} d\xi\, d\xi' + \frac{k_BT}{\zeta}K^2\sum{}''\int(1-\xi'^2)Q(m,s)Q(m,s')\Psi(s,s',\xi',\xi',0)\, d\xi'\right\} \quad (34)$$

where

$$\Psi(s,s',\xi,\xi',\tau) = e^{iK(s\xi - s'\xi')}\prod{}'' e^{-\Phi(m,s,s',\xi,\xi',\tau)} \quad (35)$$

Since $\lim\{(\partial/\partial\tau)[\mathbf{U}\exp(-\mathbf{\Lambda}^e\Theta\tau)\mathbf{U}^{-1}]\} = -\Theta\mathbf{M}^e$ and $\lim\{(\partial/\partial\tau)[\mathbf{V}\exp(-\mathbf{\Lambda}^o\Theta\tau)\mathbf{V}^{-1}]\} = -\Theta\mathbf{M}^o$, where "lim" means to take the limiting value at $\tau = 0$ of its operand, we have from eq 28a

$$-\lim\left[\frac{\partial}{\partial\tau}g_K(\xi,\xi';\tau)\right] = \Theta\sum_n n(n+1)\frac{2n+1}{2}P_n(\xi)P_n(\xi') + (D_3 - D_1)K^2\sum_n\left\{\frac{2n+1}{2}L_0(n)P_n(\xi)P_n(\xi') + \frac{2n-3}{2}L_1(n)P_n(\xi)P_{n-2}(\xi') + \frac{2n+5}{2}L_2(n)P_n(\xi)P_{n+2}(\xi')\right\} \quad (36)$$

where $L_i(n)$ are functions of n which are given in ref 16 and n runs over *all* positive integers including zero. We then have from eq 34

$$\bar{\Gamma}/K^2 = [D - \tfrac{1}{3}(D_3 - D_1)] + \frac{L^2}{12}\Theta f_1{}^*(k) + (D_3 - D_1)f_2{}^*(k) + \frac{k_BT}{\zeta L}\sum{}''a_m(k) \quad (37)$$

where

$$f_1{}^*(k) = \frac{3}{k^2}\sum_n n(n+1)(2n+1)I_{n,n}/G^1(0) \quad (38a)$$

$$f_2{}^*(k) = \sum_n[(2n+1)L_0(n)I_{n,n} + (2n-3)L_1(n)I_{n,n-2} + (2n+5)L_2(n)I_{n,n+2}]/G^1(0) \quad (38b)$$

$$a_m(k) = L\frac{1}{G^1(0)}\frac{1}{2L^2}\int d\xi'\int\int ds\, ds'\,(1-\xi'^2)Q(m,s)Q(m,s')\Psi(s,s',\xi',\xi',0) \quad (38c)$$

$$I_{n,l} = \frac{1}{4L^2}\int\int d\xi\, d\xi'\int\int ds\, ds'\, P_n(\xi)P_l(\xi')\Psi(s,s',\xi,\xi',0) \quad (38)$$

The quantity $I_{n,l}$ is the product of form factors, which is clearly seen in the stiff limit (i.e., $\langle q_m{}^2\rangle = 0$) where $I_{n,l}$ tends towards $(i)^n(-i)^l b_n(k)b_l(k)$ for even n *and* l, and zero otherwise. Thus, we have $f_1{}^*(k) \to f_1(k)$, $f_2{}^*(k) \to f_2(k)$ and $a_m(k) \to 0$ in the stiff limit; that is, eq 37 tends toward the corresponding equation for a stiff rod as given in the Introduction (Appendix B;[16] see also Appendix C[19]). Irrespective of the value of filament flexibility, it is easy to show $f_1{}^*(k) \to 0$, $f_2{}^*(k) \to {}^1/_3$ and $a_m(k) \to 0$ as $k \to 0$. As shown below, we have $f_1{}^*(k) \to 1$, $f_2{}^*(k) \to 0$, and $a_m(k) \to 1$ for $k \gg 1$.

We have the following approximation, which will be valid at $\tau \ll 1$:

$$\lim\int\left[\frac{\partial}{\partial\tau}g_K(\xi,\xi';\tau)\right]e^{iKs\xi}\prod{}'' e^{-\Phi(m,s,s',\xi,\xi',\tau)}\, d\xi \simeq \int\lim\left[\frac{\partial}{\partial\tau}g_K(\xi,\xi';\tau)e^{iKs\xi}\right]\times\lim\left[\prod{}'' e^{-\Phi(m,s,s',\xi,\xi',\tau)}\right]d\xi = \lim\left[\frac{\partial}{\partial\tau}\int g_K(\xi,\xi';\tau)e^{iKs\xi}\, d\xi\right]\times\prod{}'' e^{-\Phi(m,s,s',\xi,\xi',0)} \quad (39)$$

When we use the short-time form of $g_K{}^{\gg}(\xi,\xi';\tau)$ in eq 29

$$g_K{}^{\gg}(\xi,\xi';\tau) = [1/(4\pi\Theta\tau)]^{1/2}\exp[-(\xi-\xi')^2/(4\Theta\tau)] \qquad (\text{when } \tau \ll 1) \quad (40)$$

we have

$$\lim\left[\frac{\partial}{\partial\tau}\int g_K(\xi,\xi';\tau)e^{iKs\xi}\, d\xi\right] = -\Theta K^2 s^2 e^{+iKs\xi'} \quad (41)$$

Let us define $(L^2/12)\Theta f^*(k) \equiv (L^2/12)\Theta f_1{}^*(k) + (D_3 - D_1)f_2{}^*(k)$. Then using eq 39 and 41 we have from eq 34

$$f^*(k) \to \frac{12}{L^2}\frac{1}{G^1(0)}\frac{1}{2L^2}\int d\xi'\int\int s^2\Psi(s,s',\xi',\xi',0)\, ds\, ds' \qquad (\text{when } k \gg 1) \quad (42)$$

From eq 32 we have

$$G^1(0) = \frac{1}{2L^2}\int d\xi'\int\int\Psi(s,s',\xi',\xi',0)\, ds\, ds' \quad (43)$$

If we ignore the factors under the $\prod''$ sign in eq 35, we have $G^1(0) = (1/2)\int j_0(k\xi)^2\, d\xi = (1/L^2)\int\int j_0(K|s-s'|)\, ds\, ds'$. The *zero*th-order spherical Bessel function can be approximated as $j_0(kz) \to (\pi/k)\delta(z)$ for $k \gg 1$. In addition to this, the factors $\exp[-\Phi(m,s,s',\xi',\xi',0)]$ at $KL \gg 1$ have sharp ridges along $s = s'$ except for $\xi' = \pm 1$. Thus $\Psi(s,s',\xi',\xi',0)$ can be written as $2LG^1(0)\delta(\xi')\delta(s-s')$ for large KL's. Using this relation, we have

$$f^*(k) \to 1, \qquad a_m(k) \to 1 \qquad (\text{when } KL \gg 1) \quad (44)$$

$$\bar{\Gamma}/K^2 \to [D - \tfrac{1}{3}(D_3 - D_1)] + \frac{L^2}{12}\Theta + \frac{k_BT}{\zeta L}\sum{}''1 \quad (45)$$

The factor $\sum''1$ means the number of bending modes of motion involved in the scattering process.

We have $[D - {}^1/_3(D_3 - D_1)] = D_1$ (eq 19), $(L^2/12)\Theta = D_1$, and $k_BT/\zeta L = D_1$ in the long-rod limit (see eq 12). Thus, each mode of motion is said to contribute by D_1 to $\bar{\Gamma}/K^2$ at large KL values. In an experimentally accessible range of KL values, the $m = 2$, 3, and possibly 4 modes of motion of a long and semiflexible filament are expected to contribute to $\bar{\Gamma}/K^2$ in addition to the $m = 0$ and 1 modes.[19,23] Our previous expression for $\bar{\Gamma}/K^2$ differs from eq 45 only in D instead of $[D - {}^1/_3(D_3 - D_1)] = D_1$ (see eq C3 in ref 19).

4. Semiflexible Filaments in Semidilute Solution

In a case where there are many rods in volume L^3, the rotational motion of each rod will be severely restricted as well as the sideways translation, whereas the lengthways translation is almost free. Doi and Edwards treated the problem as follows.[18] Consider a model situation: If the rod which has been preventing the test rod from rotating (and sideways translating) diffuses a distance of order L, the constraint imposed by the rod is released and the test rod can rotate by a small amount of order a_c/L (and translating sideways by a small amount of order a_c) during a time $t_0 \simeq L^2/D_3$. This model is equivalent to the case where we assume a "cage" which confines the test rod. The cage has a radius a_c and a lifetime t_0. It is possible to imagine the free rotation of the test rod in the cage for a

very short time. However, this has been shown to have no appreciable effect on $G^1(\tau)$ (see Appendix D in ref 16). So, we assume

$$\bar{D}_1 = \bar{D}_2 \simeq a_c^2/t_0 \simeq \beta D_1, \qquad \bar{D}_3 = D_3 \tag{46a}$$

$$\bar{\Theta} \simeq (a_c/L)^2/t_0 \simeq \beta\Theta \tag{46b}$$

where $\beta = (a_c/L)^2$. Putting

$$\bar{\mu}^2 = (\bar{D}_3 - \bar{D}_1)K^2/\bar{\Theta}$$
$$(=(KL)^2(2-\beta)/(12\beta) \text{ in the long-rod limit}) \tag{47}$$

we have from eq 20

$$[\partial/\partial\tau - \bar{\Theta}(\nabla_\xi^2 - \bar{\mu}^2\xi^2)]g_K(\xi,\xi';\tau) = \delta(\xi-\xi')\delta(\tau) \tag{48}$$

Because β is very small (see below), $\bar{\mu} \gg 1$ does not necessarily mean $KL \gg 1$. The Green function in eq 48 will be given by simple replacement of μ and Θ in eq 29 with $\bar{\mu}$ and $\bar{\Theta}$, respectively. For a_c and β values, we have

$$a_c \simeq 1/(cL^2), \quad \beta \simeq 1/(cL^3)^2 \quad \text{(Doi}^{24}\text{)} \tag{49a}$$

$$a_c \simeq 1/(cL)^{1/2}, \quad \beta \simeq 1/(cL^3) \quad \text{(ours}^{16,25}\text{)} \tag{49b}$$

Since Doi considered the case of $1 \ll cL^3 \ll L/d$, he assumed a very strong constraint, and actually Doi and Edwards put $\bar{D}_1 = \bar{D}_2 = 0$.[18] We considered a rather weak constraint, $1 < cL^3 \ll L/d$. Thus, the actual β-value will lie in between the above two cases.

The mean square amplitude of the bending motion of a semiflexible filament will be given by[26]

$$\langle\delta^2\rangle = \frac{1}{L}\int_{-L/2}^{L/2}\langle\vec{r}(s,t)^2\rangle\,ds = \sum''\langle q_m^2\rangle/L = \sum''\langle\delta_m^2\rangle \tag{50}$$

Then from eq 5 and 14, we have

$$\langle\delta_m^2\rangle = 2k_BTL^3/[\epsilon\pi^4(m-\tfrac{1}{2})^4] \tag{51}$$

Using a relationship[27] $\epsilon = k_BT/(2\gamma)$, we have

$$\langle\delta_2^2\rangle^{1/2} = 0.090L(\gamma L)^{1/2} \tag{52}$$

Even for $\gamma L = 0.5$ (which may be the upper bound for γL values of the slightly bendable filament model), the root mean square amplitude of the $m = 2$ mode will be 60 nm for $L = 1$ μm and 120 nm for $L = 2$ μm. On the other hand, for $L = 1$ μm, $d = 5$ nm, and $cL^3 = 40$ (which satisfy the condition $1 < cL^3 \ll L/d$), for example, we have

$$a_c \simeq L/(cL^3) = 25 \text{ nm} \quad \text{(Doi)} \tag{53a}$$

$$a_c \simeq L/(cL^3)^{1/2} = 160 \text{ nm} \quad \text{(ours)} \tag{53b}$$

The above-mentioned values of $\langle\delta_2^2\rangle^{1/2}$ and a_c suggest that the bending motion of the semiflexible filament is slightly restricted in the Doi–Edwards model but almost free in our model. We consider the so-called reptile motion of filaments and, for simplicity of discussion, assume that the bending motion is free from surrounding filaments. Then from eq 29 and 32, we have the expression for $G^1(\tau)$ provided that we replace D's, μ, and Θ by $\bar{D}$'s, $\bar{\mu}$, and $\bar{\Theta}$, respectively. When $\bar{\mu}$ is sufficiently large, we have an approximate form. From eq 29b, we have[18]

$$g_K^{\gg}(\xi,\xi';\tau) = \text{sech}\,(\bar{\mu}\bar{\Theta}\tau)\,\exp[-\bar{\mu}\xi^2\tanh(\bar{\mu}\bar{\Theta}\tau)]\delta(\xi-\xi') \tag{54}$$

where use was made of an approximation

$$\exp\left[-\frac{\bar{\mu}}{4}(\xi-\xi')^2/\tanh(\bar{\mu}\bar{\Theta}\tau)\right] = \left[\frac{4\pi}{\bar{\mu}}\tanh(\bar{\mu}\bar{\Theta}\tau)\right]^{1/2}\delta(\xi-\xi') \tag{55}$$

Originally, this approximation was derived for $\bar{\mu} \gg 1$ *and* $KL \leq 3$, but we showed that it is valid for arbitrary values of KL provided that the β-value is sufficiently small (see Appendix E in ref 16). Then we have

$$J(s,s',\tau) = \exp(-\bar{D}_1K^2\tau)\,\text{sech}\,(\bar{\mu}\bar{\Theta}\tau)\left[\frac{1}{2}\int_{-1}^{1}e^{iK(s-s')\xi}\times \exp[-\bar{\mu}\xi^2\tanh(\bar{\mu}\bar{\Theta}\tau)]\prod''\exp[-\Phi(m,s,s',\xi,\xi,\tau)]\,d\xi\right] \tag{56}$$

The limiting form of the first cumulant is given by

$$\bar{\Gamma}/K^2 \to \beta D_1 + \beta(L^2/12)\Theta + D_1\sum''1 \quad (\text{when } KL \gg 1) \tag{57}$$

(Equation 56 also gives eq 57 with missing $\beta(L^2/12)\Theta$, which solely comes from the assumption $\delta(\xi-\xi')$ in eq 55.) Since β is very small, the translational and rotational modes of motion contribute very little to $\bar{\Gamma}/K^2$. Even in an experimentally accessible range of KL values, the decay of $G^1(\tau)$ mostly comes from the bending motion in the case of very long and semiflexible filaments in semidilute solution. It should be noted, however, that the integral part in eq 56 (after further integration over s and s') decays to a nonzero value depending on γL and KL values. For this reason, $G^1(\tau)$ has a very long tail which decays to zero as $\exp(-\bar{D}_1K^2\tau)\,\exp(-\bar{\mu}\bar{\Theta}\tau)$.

Since $\bar{\mu}\bar{\Theta} = (D_3K^2 \times \bar{\Theta})^{1/2}$, the trajectory of the motion of the filament is determined by a combined process of the free lengthways translation, very small angle steps, and bending motion; that is, the trajectory is just the trace of a *reptile* motion. Fluorescence-dye-labeled F-actin (~10 μm long, ca. 10 μg/mL) can directly be observed under a video-enhanced fluorescence microscope. Using this technique, one can observe a reptile motion of labeled F-actin in a semidilute solution of unlabeled F-actin (Honda, H.; Nagashima, H.; Asakura, S., personal communication).

5. Numerical Simulation and Discussion

We would like to present some numerical simulation results in order to visualize the theoretical results given above.

1. Semiflexible Filament in the Dilute Regime. In terms of the new variables

$$\eta = \frac{\xi+\xi'}{2}, \qquad \eta' = \frac{1}{\kappa}\frac{\xi-\xi'}{2} \qquad \text{with } \kappa^2 = \tanh(\mu\Theta\tau)/\mu \tag{58}$$

eq 29b is written as

$$g_K^{\gg}(\xi,\xi';\tau)\,d\xi\,d\xi' = \frac{1}{\pi^{1/2}}\,\text{sech}\,(\mu\Theta\tau)e^{-(\mu\kappa\eta)^2}e^{-\eta'^2}\,d\eta\,d\eta' \tag{59}$$

From eq 16, 32, 33, and 59, we have

$$G^1(\tau) = G_{D\Theta}(\tau)\frac{1}{\pi^{1/2}}\frac{1}{L^2}\int\int_{-L/2}^{L/2}ds\,ds'\int_{-1}^{1}d\eta\int_0^{(1-|\eta|)/\kappa}d\eta' e^{-(\mu\kappa\eta)^2}e^{-\eta'^2}e^{iK(s-s')\eta}e^{iK(s+s')\kappa\eta'}\prod_m''\exp[-\Phi(m,s,s',\xi(\eta,\eta'),\xi'(\eta,\eta'),\tau)] \quad (\text{when } \mu \gg 1) \tag{60}$$

$$G_{D\Theta}(\tau) = G_D(\tau)\,\text{sech}\,(\mu\Theta\tau) \tag{61}$$

If we assume $\xi = \xi'$ in eq 33, we have from eq 60 (see Appendix A in ref 16)

$$G^1(\tau) = G_{D\Theta}(\tau)\frac{1}{\pi^{1/2}}\frac{2}{L^2}\int\int_{-L/2}^{L/2}ds\,ds'\int_0^1 d\eta\, e^{-(\mu\kappa\eta)^2}\prod''\exp[-\Phi(m,s,s',\eta,\eta,\tau)]\cos[K(s-s')\eta]e^{-[K(s+s')\kappa/2]^2} \tag{62}$$

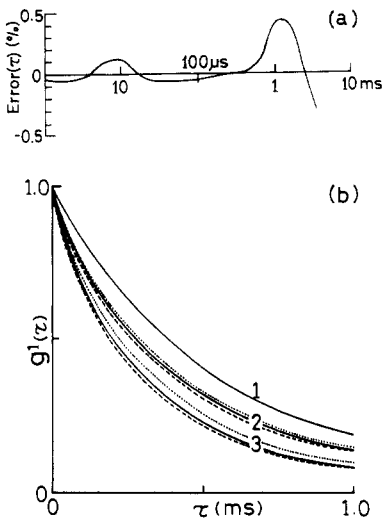

Figure 2. Simulation of correlation functions based on the harmonic oscillator model. (a) Error (τ) versus log τ indicating the negligible effect of difference between ξ and ξ' in $\Phi(m,s,s',\xi,\xi',\tau)$. $L = 1.0$ μm, $D = 1.32 \times 10^{-8}$ cm^2/s at 5 °C, $D_3 = 2D_1$, $\Theta = 12D_1/L^2$, $K^2 = 10 \times 10^{10}$ cm^{-2} ($KL \simeq 32$), and $\gamma L = 0.5$. Here and hereafter, internal terms up to $m = 8$ were taken in computation (see ref 19). Error $(\tau) \equiv [g^1(\tau)_{\text{eq 60}} - g^1(\tau)_{\text{eq 62}}]/g^1(\tau)_{\text{eq 62}}$. (b) Some examples of simulated correlation functions based on eq 62. Parameter values are the same as in (a) except for $\gamma L = 0.0$ (curve 1), 0.1 (curve 2), and 0.5 (curve 3). (—) Without preaverage; (··) with preaverage ($\Delta = 0$); (- - -) with preaverage ($\Delta = 1$).

The fourfold integration in eq 60 can be carried out in two steps: integration over η' and then integration over s, s', and η. Since the integrand at the first step has appreciable values only in the neighborhood of $\eta' = 0$, subroutines based on a double-exponential formula[28] are used at this step. The threefold integration at the second step is carried out with an adaptive N-dimensional quadrature subroutine,[29] which is also used for other multifold integration. The multifold integration will usually be carried out with error tolerance of 0.1%.

From eq 14, 50, and 51 and the relationship $\langle q_m^2\rangle/\tau_m = 2k_BT/\zeta$, we have $\tau_2 = 0.0486(\gamma L)/\Theta$. From the Einstein relation $\langle(\xi - \xi')^2\rangle = 2\Theta\tau$, we have at time τ_2, $\langle\xi\xi'\rangle = \langle\xi'^2\rangle \exp[-0.0486(\gamma L)]$. That is, ξ changes very little from the initial value ξ' during the time interval τ_2. This suggests that the difference between ξ and ξ' in eq 33 is not very important. To see this, numerical results based on eq 60 were compared with those based on eq 62. So far as we have studied for $L = 1$ μm, $K^2 = 10 \times 10^{10}$ cm^{-2} ($\mu^2 = 83.3$, $KL \simeq 32$), and $\gamma L = 0.0$ (rod), 0.1, and 0.5, we observed $|g^1(\tau)_{\text{eq 60}} - g^1(\tau)_{\text{eq 62}}| \leq 0.0005$ (see Figure 2a). Next, the effect of ξ in $\Phi(m,s,s',\xi,\xi,\tau)$ on $G^1(\tau)$ was examined, which was not explicitly considered in our old model.[19] By defining $\Phi(m,s,s',\xi,\xi,\tau) = (1 - \xi^2)\Phi_0(m,s,s',\tau)$, we have

$$\prod{}''\exp[-\Phi(m,s,s',\xi,\xi,\tau)] = \sum_{p=0}\frac{1}{p!}[-\sum{}''\Phi_0(m,s,s',\tau)]^p(1 - \xi^2)^p \quad (63)$$

When we take the preaverage of $(1 - \xi^2)^p$ independently of the average over ξ with weight $\exp(iKs\xi)g_K(\xi,\xi';\tau)$, we have

$$\langle\prod{}''\exp[-\Phi(m,s,s',\xi,\xi,\tau)]\rangle_\xi = \prod{}''\exp\left[-\frac{2+\Delta}{3}\Phi_0(m,s,s',\tau)\right] \quad (64)$$

where use was made of $\int(1 - \xi^2)^p\,d\xi = (2p)!!/(2p + 1)!!$ The value of Δ depends on the value of $\sum{}''\Phi_0(m,s,s',\tau)$ and is in the range $0 < \Delta < 1$. Figure 2b shows $G^1(\tau)$ based on eq 62 with ξ in Φ (solid lines), $\Delta = 0$ (dotted lines), and $\Delta = 1$ (dashed lines). For the present parameter values, $L = 1$ μm and $\mu^2 = 83.3$ ($KL \simeq 32$), $G^1(\tau)$ with $\Delta = 1$ is closer to the exact value at $\gamma L = 0.5$, but the $G^1(\tau)$'s with $\Delta = 0$ and 1 deviate by nearly the same amount but in opposite directions from the exact value at $\gamma L = 0.1$.

For intermediate μ^2 values, we have to use $g_K(\xi,\xi';\tau)$ in eq 28 for the computation of $G^1(\tau)$. Assuming again $\xi = \xi'$ in eq 33, we have from eq 32

$$G^1(\tau) = G_D(\tau)\frac{1}{2L^2}\int\int_{-L/2}^{L/2}ds\,ds'\int_{-1}^{1}d\xi\prod_m{}''\exp[-(1 - \xi^2)\Phi_0(m,s,s',\tau)]\sum_n\sum_l(2l + 1)(-i)^l\mathbf{W}_{nl}(\tau)j_l(Ks')P_n(\xi)e^{iKs\xi} \quad (65)$$

where (see eq 27)

$$\begin{aligned}\mathbf{W}_{nl}(\tau) &= [\mathbf{U}\exp(-\Lambda^e\Theta\tau)\mathbf{U}^{-1}]_{nl} \quad \text{for even } n \text{ and } l\\ &= [\mathbf{V}\exp(-\Lambda^o\Theta\tau)\mathbf{V}^{-1}]_{nl} \quad \text{for odd } n \text{ and } l\\ &= 0 \quad \text{for mixed } n \text{ and } l\end{aligned} \quad (66)$$

If we assume eq 64, we have from eq 65

$$G^1(\tau) = G_D(\tau)\frac{1}{L^2}\int\int_{-L/2}^{L/2}ds\,ds'\prod_m{}''\exp\left[-\frac{2+\Delta}{3}\Phi_0(m,s,s',\tau)\right]\sum_n\sum_l(2l + 1)(i)^n(-i)^l\mathbf{W}_{nl}(\tau)j_n(Ks)j_l(Ks') \quad (67)$$

In eq 65 and 67, if the summation over l is limited only to $l = n$ (diagonal) and $n \pm 2$ (the first off-diagonals) (see ref 16), the integrands in these equations become very simple.

In order to compare the present result with our previous one, let us assume $D_3 = D_1$ (isotropic translation). For $\mu^2 = 0$, we have from eq 65 and 67

$$G^1(\tau) = e^{-DK^2\tau}\frac{1}{2L^2}\int\int_{-L/2}^{L/2}ds\,ds'\int_{-1}^{1}d\xi\prod_m{}''\exp[-(1 - \xi^2)\Phi_0(m,s,s',\tau)]\sum_n(2n + 1)(-i)^nj_n(Ks')P_n(\xi)e^{iKs\xi}e^{-n(n+1)\Theta\tau} \quad (68)$$

and

$$G^1(\tau) = e^{-DK^2\tau}\frac{1}{L^2}\int\int_{-L/2}^{L/2}ds\,ds'\prod_m{}''\exp\left[-\frac{2+\Delta}{3}\Phi_0(m,s,s',\tau)\right]\sum_n(2n + 1)j_n(Ks)j_n(Ks')e^{-n(n+1)\Theta\tau} \quad (69)$$

Equation 69 with $\Delta = 1$ is just what we have considered in our previous paper (see Appendix D in ref 19). In eq 68 and 69, n runs over both even and odd positive integers including zero. Figure 3 shows some examples of simulated $G^1(\tau)$'s based on eq 69 with $\Delta = 1$ and $\gamma L = 0.0$ (for rod, curve 1), 0.1 (curves 2), and 0.5 (curves 3). Instead of $\exp(-DK^2\tau)$ in eq 69, we intentionally adopted $\exp(-D_1K^2\tau)$ [$\equiv G_D(\tau)$] with $D_1 = (3/4)D$ (see below for reason). The dashed lines show the results for only even-n terms in eq 69 (for $\gamma L \neq 0$). Even for $\gamma L = 0.1$, the odd-n terms in eq 69 (and also eq 65, 67, and 68) have a big contribution to $G^1(\tau)$ at larger KL values.

Figure 4 shows some examples of simulated correlation functions based on eq 65 with $D_3 = 2D_1$ (solid lines) and on eq 67 with $D_3 = 2D_1$ and $\Delta = 0$ (dotted lines) or $\Delta = 1$ (dashed lines). These results indicate that (i) at low angles and small γL values where the effect of the filament flexibility on $G^1(\tau)$ is small, eq 65 and 67 with $\Delta = 0$ give almost the same $G^1(\tau)$'s, (ii) at high angles and large γL values where the effect of the filament flexibility on $G^1(\tau)$ is large, eq 67 with $\Delta = 1$ gives $G^1(\tau)$'s close to those given

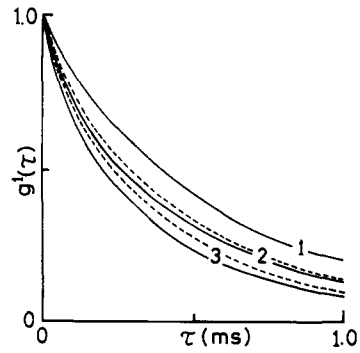

Figure 3. Some examples of simulated correlation functions based on eq 69. $L = 1.0\ \mu m$, $D = 1.32 \times 10^{-8}\ cm^2/s$ at 5 °C, $D_3 = 2D_1$, $\Theta = 12D_1/L^2$, $K^2 = 10 \times 10^{10}\ cm^{-2}$, $\Delta = 1$, and $\gamma L = 0.0$ (curve 1), 0.1 (curve 2), and 0.5 (curve 3). (- - -) Only even-n terms; (—) both even- and odd-n terms.

by eq 65, and (iii) at intermediate angles and/or γL values, eq 65 gives $G^1(\tau)$ in between those given by eq 67 with $\Delta = 0$ and 1. To see these features more clearly, let us define

$$\text{Dev}\ (\Delta) = g^1(\tau) - g^1(\tau)_\Delta \tag{70a}$$

$$\overline{\text{Dev}} = g^1(\tau) - [g^1(\tau)_{\Delta=0} + g^1(\tau)_{\Delta=1}]/2 \tag{70b}$$

where $g^1(\tau)$ is the normalized correlation function given by eq 65 and $g^1(\tau)_\Delta$ is that given by eq 67 with $\Delta = 0$ or 1. For $g^1(\tau)$'s in Figure 4, Dev (Δ) and $\overline{\text{Dev}}$ are plotted in Figure 5. The quantity |Dev (0)| is less than 1% for the first three cases from the top (up to $KL \simeq 14$). For $KL > 14$, Dev (1) becomes smaller than |Dev (0)|, but Dev (1) amounts to 2% at the maximum. On the other hand, $\overline{\text{Dev}}$ is less than 1% for all K^2 values studied. If we compute $G^1(\tau)$'s based on eq 67 with $\Delta = 0.5$, for example, Dev (0.5) would be less than 1% for all K^2 values. (Mathematically speaking, $\Delta \to 1$ occurs only when $KL \to \infty$.) Although both |Dev (0)| and Dev (1) are not very large, their quick rise affects the value of the initial decay rate of $G^1(\tau)$ as shown below.

We also computed $G^1(\tau)$'s based on eq 68 and 69. The results showed trends similar to those given in Figures 4 and 5. Using the simulated $G^1(\tau)$'s, we computed the first cumulant $\bar{\Gamma}$, and $\bar{\Gamma}/K^2$ is plotted in Figure 6. For $KL \leq 10$, $\bar{\Gamma}/K^2$ for $\Delta = 0$ (□,■) coincides with the exact one (○,●). For $KL > 10$, the difference between $\bar{\Gamma}/K^2$ for $\Delta = 1$ (△,▲) and the exact one (○,●) is about $D_1/3$ at $\gamma L = 0.5$ and less than $D_1/6$ at $\gamma L = 0.1$. These differences are very much reduced if we put $\Delta = 0.5$. (See inset in Figure 6, where dev (Γ) $\equiv [\bar{\Gamma}_{\text{eq 67 with } \Delta=0.5} - \bar{\Gamma}_{\text{eq 65}}]/K^2$. The dev ($\Gamma$) for eq 68 and 69 has almost the same values as those shown here.) When $\bar{\Gamma}/K^2$ of $G^1(\tau)$'s based on eq 68 and 69 are plotted with displacement by $-D/4 \equiv -D_1/3$, the corresponding values (i.e., each pair of open and closed symbols in Figure 6) agree fairly well for $KL \geq 10$. This is a natural consequence of putting $\xi = \xi'$ in $\Phi(m,...)$. Due to this, anisotropic translation of a semiflexible filament has no direct effect on contribution to $G^1(\tau)$ from bending modes of motion. There is, however, an indirect effect of anisotropic translation through terms $l \neq n$ in eq 65 and 67, but this effect is dominant at $KL \leq 10$ where filament flexibility has little effect on $G^1(\tau)$. Equations 68 and 69 after simple replacement of $\exp(-DK^2\tau)$ with $G_D(\tau)$, or with $G_D^*(\tau)$ in eq 71c below, give fairly nice $G^1(\tau)$'s for semiflexible filaments at $KL \geq 10$. To see this, let us define

$$\text{dev} = g^1(\tau)_{\text{eq 68 with } G_D(\tau)} - g^1(\tau)_{\text{eq 65}} \tag{71a}$$

$$\text{dev}^* = g^1(\tau)_{\text{eq 68 with } G_D^*(\tau)} - g^1(\tau)_{\text{eq 65}} \tag{71b}$$

$$G_D^*(\tau) = \exp[-\{D - \tfrac{1}{3}(D_3 - D_1)(1 - 3f_2(k))\}K^2\tau] \tag{71c}$$

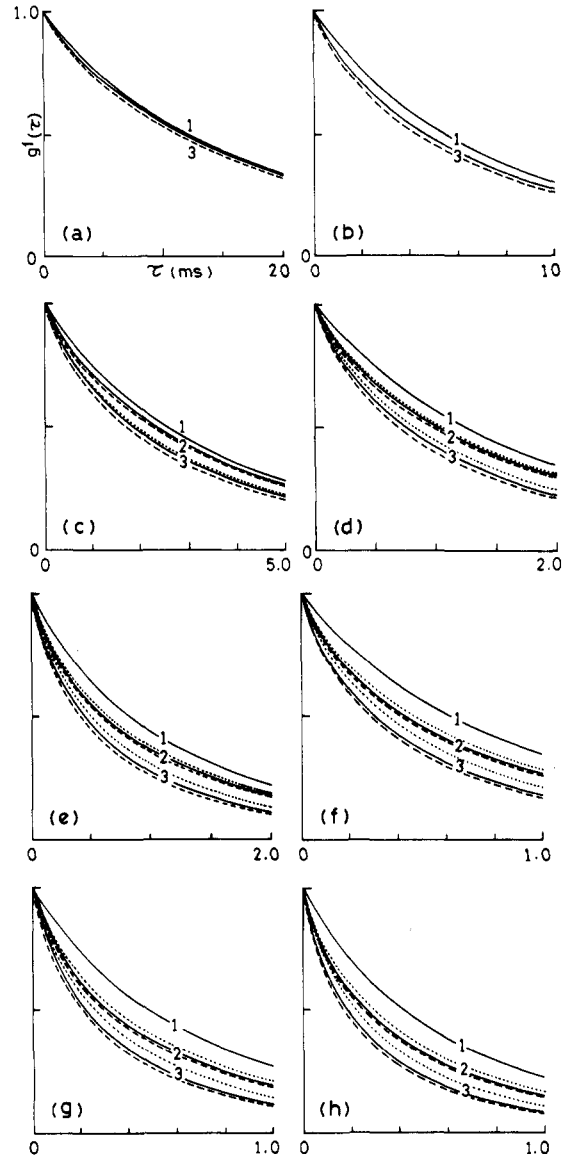

Figure 4. Some examples of simulated correlation functions at different scattering angles. $L = 1.0\ \mu m$, $D = 1.32 \times 10^{-8}\ cm^2/s$ at 5 °C, $D_3 = 2D_1$, $\Theta = 12D_1/L^2$, and $\gamma L = 0.0$ (curves 1), 0.1 (curves 2), and 0.5 (curves 3). (—) Based on eq 65; (···) and (- - -) based on eq 67 with $\Delta = 0$ and 1, respectively. (a) $K^2 = 0.5 \times 10^{10}\ cm^{-2}$ ($KL = 7.07$); (b) 1.0×10^{10} (10); (c) 2.0×10^{10} (14.1); (d) 4.0×10^{10} (20); (e) 6.0×10^{10} (24.5); (f) 8.0×10^{10} (28.3); (g) 10×10^{10} (31.6); (h) 11.7×10^{10} (34.2). In (a) and (b), curves for $\gamma L = 0.1$ are not shown in order to avoid complexities. The dotted curves for $\gamma L = 0.5$ in (a) and (b) and for $\gamma L = 0.1$ in (c) are the same as the corresponding solid lines within the width of each line.

(The quantity $f_2(k)$ is the limiting value of $f_2^*(k)$ in eq 38b at $\gamma L \to 0$; see ref. 16 for its numerical values.) Figure 7 shows some examples of dev and dev*. For rods ($\gamma L = 0.0$, dotted lines), dev* $\simeq 0$ except for the first one at $K^2 = 0.5 \times 10^{10}\ cm^{-2}$ ($KL = 7.07$). Even at $\gamma L = 0.5$ (dashed lines), dev* is not very large. The difference between dashed and dotted lines mainly comes from the indirect effect of anisotropic translation mentioned above.

A method to estimate the γL value of a semiflexible filament will be provided by comparing the experimental $\bar{\Gamma}/K^2$ with simulated ones at varied γL values.[19,23] To do this, the fact that the fourfold integration over s, s', ξ, and ξ' for simulation of $G^1(\tau)$ can be reduced to the threefold integration over s, s', and ξ with a very high accuracy is very important to save computation time. As an approximate method, we can even use two-fold integration such

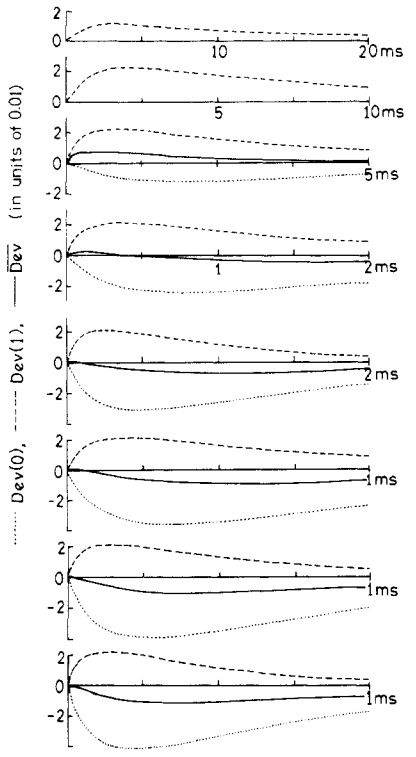

Figure 5. Deviations, Dev (Δ) and $\overline{\text{Dev}}$, at differeent scattering angles. Dev (0), Dev (1), and $\overline{\text{Dev}}$ (see eq 70 for their definition) were computed by using $g^1(\tau)$'s for $\gamma L = 0.5$ in Figure 4. From top to bottom, $K^2 = 0.5 \times 10^{10}$, 1.0×10^{10}, 2.0×10^{10}, 4.0×10^{10}, 6.0×10^{10}, 8.0×10^{10}, 10.0×10^{10}, and 11.7×10^{10} cm^{-2}.

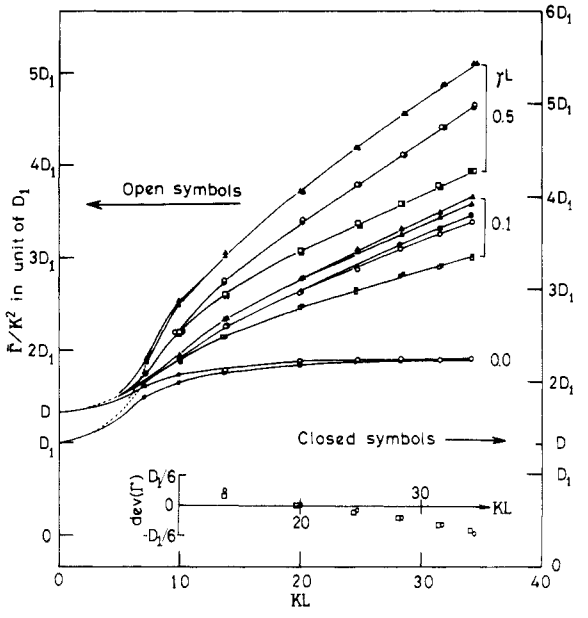

Figure 6. $\bar{\Gamma}/K^2$ vs. KL relationships of simulated correlation functions. $L = 1.0$ μm, $D = 1.32 \times 10^{-8}$ cm^2/s at 5 °C, $D_3 = 2D_1$, $\Theta = 12D_1/L^2$, and $\gamma L = 0.0$, 0.1, and 0.5. (○) Based on eq 65; (□) eq 67 with $\Delta = 0$; (△) eq 67 with $\Delta = 1$; (●) eq 68; (■) eq 69 with $\Delta = 0$; (▲) eq 69 with $\Delta = 1$. The inset shows dev (Γ) $\equiv [\bar{\Gamma}_{\text{eq 67 with } \Delta = 0.5} - \bar{\Gamma}_{\text{eq 65}}]/K^2$ for $\gamma L = 0.1$ (□) and 0.5 (○).

as eq 67 or 69 with replacement of $\exp(-DK^2\tau)$ by $G_D(\tau)$ or $G_D^*(\tau)$. In this case, an analysis for $\Delta = 1$ gives the lower bound of the γL value and an analysis for $\Delta = 0$ gives the upper bound of the γL value. For the present particular choice of the parameter values, the assumption of $\Delta = 0.5$ gives a sufficiently accurate result. Even our old model gives a rough estimate of the γL value.

2. Semiflexible Filaments in the Semidilute Regime. Simulation of $G^1(\tau)$ in this regime was made for L

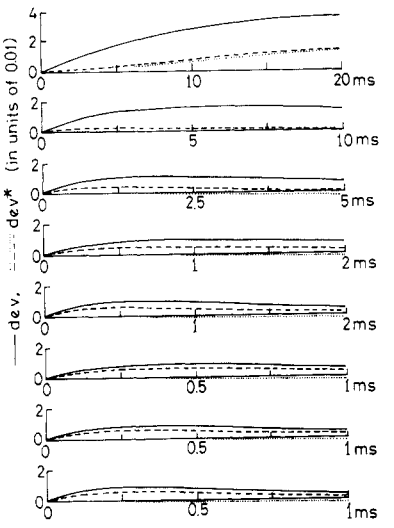

Figure 7. Deviations, dev and dev*, at different scattering angles. $L = 1.0$ μm, $D = 1.32 \times 10^{-8}$ cm^2/s at 5 °C, $D_3 = 2D_1$, $\Theta = 12D_1/L^2$, and $\gamma L = 0.0$ (···) and 0.5 ((—) and (---)). For definition of dev and dev*, see eq 71. From top to bottom, $K^2 = 0.5 \times 10^{10}$, 1.0×10^{10}, 2.0×10^{10}, 4.0×10^{10}, 6.0×10^{10}, 8.0×10^{10}, 10.0×10^{10}, and 11.7×10^{10} cm^{-2}.

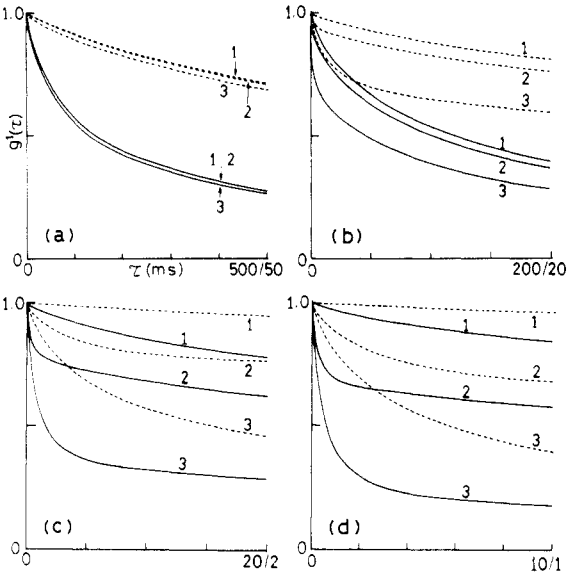

Figure 8. Some examples of simulated correlation functions in the semidilute regime. $L = 1.0$ μm, $D = 1.32 \times 10^{-8}$ cm^2/s at 5 °C, $D_3 = 2D_1$, $\Theta = 12D_1/L^2$, $\beta = 1/1600$, and $\gamma L = 0.0$ (curves 1), 0.1 (curves 2), and 0.5 (curves 3). From (a) to (d), $K^2 = 0.5 \times 10^{10}$, 2.0×10^{10}, 6.0×10^{10}, and 10.0×10^{10} cm^{-2}, respectively. The time axis in each figure is scaled in two ways; for example, 500/50 in (a) means 500 ms for solid curves and 50 ms for dashed curves. Simulation was made by use of eq 56.

$= 1.0$ μm, $D = 1.32 \times 10^{-8}$ cm^2/s (at 5 °C), $D_3 = 2D_1$, $\Theta = 12D_1/L^2$, $\gamma L = 0.0$, 0.1, and 0.5, and $\beta = 1/1600$ (eq 49a) and 1/40 (eq 49b). For $\beta = 1/1600$, $\bar{\mu}^2 = (KL)^2/(6\beta)$ is so large that eq 55 holds[16] and we can use eq 56. For $\beta = 1/40$, on the other hand, eq 55 does not hold[16] and we have to use eq 62 after replacement of D's, Θ and μ with $\bar{D}$'s, $\bar{\Theta}$, and $\bar{\mu}$, respectively. The assumption of $\xi = \xi'$ in $\Phi(m,s,s',...)$ in eq 33 is valid in any case because $\bar{\Theta} \ll \Theta$.

Figure 8 shows some examples of simulated results for $\beta = 1/(cL^3)^2 = 1/1600$. The solid lines show a long-time behavior of $G^1(\tau)$ whereas the dashed lines show a short-time behavior (the first one-tenth of the delay time) of corresponding $G^1(\tau)$ shown by the solid lines. Compared with the case of a rigid rod ($\gamma L = 0.0$), $G^1(\tau)$ for a semiflexible filament ($\gamma L \neq 0$) shows an initial fast decay

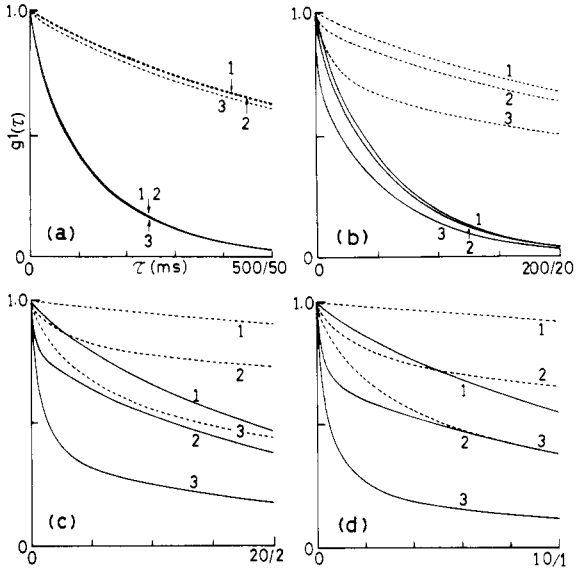

Figure 9. Some examples of simulated correlation functions in the semidilute regime. Except for $\beta = 1/40$, all the conditions are the same as those in Figure 8. Simulation was made by use of eq 62.

followed by a very slow decay. The initial fast decay comes from the contribution of bending motions of the semiflexible filament. The very slow decay in the long-time region mainly comes from a time behavior of $G_{D\bar{\Theta}}(\tau) = \exp(-\beta D_1 K^2 \tau)$ sech $(\bar{\mu}\bar{\Theta}\tau)$ in eq 61. At $K^2 = 0.5 \times 10^{10}$ cm^{-2} (Figure 8a), $\exp(-\beta D_1 K^2 \tau)$ decays to 0.98, sech $(\bar{\mu}\bar{\Theta}\tau)$ to 0.91, and hence $G_{D\bar{\Theta}}(\tau)$ to 0.89 at $\tau = 500$ ms. On the other hand, $G_D(\tau) = \exp(-D_1 K^2 \tau)$ in eq 19 (for a dilute solution) decays to 0.78 even at $\tau = 5$ ms.

Figure 9 shows some examples of simulated results for $\beta = 1/(cL^3) = 1/40$. The solid and dashed lines have the same meanings as those in Figure 8. The general trend of the time behavior of $G^1(\tau)$ is very similar to the corresponding one in Figure 8. A marked difference between $G^1(\tau)$'s in Figures 8 and 9 appears in the long-time behavior; the value of $G^1(\tau)$ for each set of parameter values is smaller in Figure 9 than in Figure 8. This mainly comes from a faster decay of $G_{D\bar{\Theta}}(\tau)$ for smaller β values. For $\beta = 1/40$ and $K^2 = 0.5 \times 10^{10}$ cm^{-2} (Figure 9a), $\exp(-\beta D_1 K^2 \tau)$ decays to 0.54, sech $(\bar{\mu}\bar{\Theta}\tau)$ to 0.057, and hence $G_{D\bar{\Theta}}(\tau)$ to 0.031 at $\tau = 500$ ms.

It is a characteristic feature of a semiflexible filament in a semidilute solution that $G^1(\tau)$ shows an initial fast decay followed by a very slow one. Because of the following difficulties, however, $G^1(\tau)$'s shown in Figures 8 and 9 should be regarded to show qualitative features. The original Doi–Edwards model assumes $\bar{\Theta} = k_1\Theta/(cL^3)^2$, where k_1 is a proportionality constant (expected to be within an order of 10; cf. eq 46). Let $c^* = M_w/NL^3$ (M_w is molecular weight and N is the Avogadro number) and c_p be the concentration of rods in units of g/mL. Since $cL^3 = (c_p/c^*)$, we have $\Theta/\bar{\Theta} = (1/k_1)(c_p/c^*)^2$. From experimental data for rodlike viruses by transient electric birefringence measurements,[30] we can estimate the k_1 values to be about 5000 for M-13-WT ($L = 0.892$ μ, $d = 8.5$ nm, and $M_w = 1.6 \times 10^7$) and about 17 000 for M-13-T$_n$3-15 ($L = 1.58$ μm, $d = 8.5$ nm, and $M_w = 2.28 \times 10^7$). Both values are very much larger than predicted. The same situation has been reported also for other cases. From depolarized light-scattering measurements,[31] the k_1 values are reported to be 1070, 1170, and 1786 for PBLG with $M_w = 150\,000$, 170 000, and 210 000, respectively. From dynamic electric birefringence measurements,[25] the low relaxation frequency $\bar{f}_L$ was obtained to be 77 Hz, resulting again in a difference of 700 times. Although almost complete c^{-2} and fairly good L^{-9} dependences are confirmed in the cases cited above, the absolute value of $\bar{\Theta}$ is several orders of magnitude larger than predicted. Another problem is specific to polarized light scattering. For a very long filament, $L = 1$ μm and $cL^3 = 64$, for example, correspond to 4 filaments/1 μm or 250 nm/filament. This means that a filament is confined in a cage with a diameter of about 250 nm. The sideways translation of the filament in the cage could be detected, because we have $1/K = 100$ nm even for such a low angle as $K^2 = 1 \times 10^{10}$ cm^{-2}. That is, even if $\bar{D}_1 = k_2 D_1/(cL^3)^2$ is assumed instead of $\bar{D}_1 = 0$ in the original Doi–Edwards model, the proportionality constant k_2 would have a very large value as k_1 does. Our alternatives, $\bar{\Theta} = k_1'\Theta/(cL^3)$ and $\bar{D}_1 = k_2' D_1/(cL^3)$ (eq 49b), still have problems; both k_1' and k_2' will have a value much larger than 10. Unexpected light-scattering results[32] for M-13-WT might come from these reasons.

3. Application. Dilute Solution. As an application of the model, the experimental result of fd virus is first considered. The translational diffusion constant from dynamic light-scattering measurements at low angles and the rotational diffusion constant from transient electric birefringence measurements were, after extrapolation to infinite dilution, $D_{25°C} = (2.58 \pm 0.04) \times 10^{-8}$ cm^2/s and $\Theta_{20°C} = (20.9 \pm 0.3)$ s^{-1}, respectively, which corresponded to a virus length of (895 ± 20) nm and a diameter of (9 ± 1) nm.[33] The dynamic light-scattering data over a wide range of K^2 values are available only at a concentration of 0.27 mg/mL,[10] which corresponds to $cL^3 \simeq 7$ if $M_w = 1.64 \times 10^7$ is assumed.[33] This concentration is in neither a dilute nor a semidilute regime. We have to take account of a slight overlap of filaments at this concentration. However, our model in a dilute regime will be applied, because electric birefringence measurements showed very little change in the Θ value up to this concentration.[30,33]

After T/η correction, we have $D_{5°C} = 1.41 \times 10^{-8}$ cm^2/s and $\Theta_{5°C} = 13.1$ s^{-1}. By use of Broersma's revised formulas quoted in ref 33, we have $D_1 = 1.19 \times 10^{-8}$ cm^2/s, $D_3 = 1.87 \times 10^{-8}$ cm^2/s, and $D_3 - D_1 = 0.68 \times 10^{-8}$ cm^2/s at 5 °C. The ζ value can be estimated from the experimental Θ values as before;[19] i.e., $k_BT/\zeta L = (L^2/12)\Theta$, which is equivalent to $D = [(4/3)k_BT/\zeta L]\Phi(p)$ in eq A11 of ref 19. For these parameter values, the field correlation functions were computed by use of eq 65. Simulated correlation functions were then least-squares fitted to the second-order cumulant expansion formula. The results are shown in Figure 10a, where the dashed lines show our previous results in ref 19. Due to anisotropy in translational diffusion, the $\bar{\Gamma}$ values for rods ($\gamma L = 0.0$) are smaller than the previous ones. The experimental $\bar{\Gamma}$ values are substantially larger than the simulated ones for $\gamma L = 0.0$ in the dilute regime. Thus, we have to take account of the filament flexibility. For $\gamma L = 0.1$, the present model can simulate the behavior of experimental $\bar{\Gamma}$ values. Because of the difference in the definition of γ,[27] the present value of $\gamma L = 0.1$ *should read* 0.15 if the γL values are compared between the present and the previous results. This trouble is eliminated when ϵ values are compared. Due to the effect of anisotropy in translational diffusion, the present model requires a little larger flexibility (compared with the previous model) in order to simulate the experimental $\bar{\Gamma}$ vs. K^2 relationship of fd virus. The present analysis and the previous one strongly suggest the nonrigid nature of this virus. Actually, images of this virus particle on electron micrographs are irregularly curved.

For a rod with a very large axial ratio $p = L/d$, the end-effect corrections in the theoretical expressions of

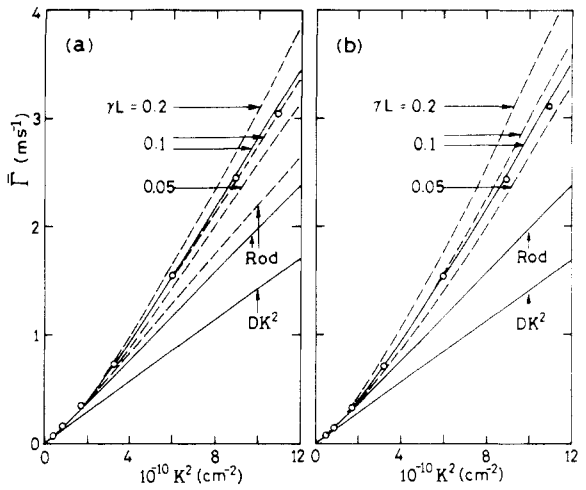

Figure 10. $\bar{\Gamma}$ vs. K^2 relationships of simulated correlation functions. (a): (O) Experimental results for fd virus at a concentration of 0.27 mg/mL (from ref 10); (—) simulated results by use of eq 65 with $D = 1.41 \times 10^{-8}$ cm^2/s, $D_1 = 1.19 \times 10^{-8}$ cm^2/s, $D_3 = 1.87 \times 10^{-8}$ cm^2/s, $\Theta = 13.1$ s^{-1}, $L = 0.895$ μm, and temperature = 5 °C; (- - -) previous results[19] for $D = 1.41 \times 10^{-8}$ cm^2/s, $\Theta = 13.1$ s^{-1}, $L = 0.895$ μm, and temperature = 5 °C. In both cases, the ζ value was estimated from the experimental Θ value (see text). (b): (O) and (—) Same as those in (a); (- - -) the parameter values were the same as those for (—) except that the ζ value was estimated from the theoretical D_1 value (see text).

diffusion constants can be neglected, and the friction constant ζ for a bending motion can be equally estimated from relationships $k_BT/\zeta L = L^2\Theta/12 = D_1 = (3/4)D$. In an actual case, the p value is not extremely large ($p \simeq 100$ for fd virus), so that the end-effect corrections are not negligibly small. For fd virus at 5 °C, we have $\zeta L = 4.39 \times 10^{-6}$, 4.36×10^{-6}, and 3.23×10^{-6} (erg·s)/cm^2 for $k_BT/\zeta L = L^2\Theta/12$, $D = [(4/3)k_BT/\zeta L]\Phi(p)$, and $k_BT/\zeta L = D_1$, respectively. The first two values are essentially the same but substantially larger than the last one. We do not know which ζ value should be adopted for the present problem, although we feel that the first two values are more appropriate than the last one. Figure 10b shows simulated results for the ζL values from $k_BT/\zeta L = L^2\Theta/12$ (solid lines) and from $k_BT/\zeta L = D_1$ (dashed lines), keeping other parameters unchanged. For a quantitative analysis of experimental results, a theoretical modeling on the ζ value is necessary.[34]

Semidilute Solution. Maguire reported polarized light-scattering data of semidilute solutions (up to $cL^3 = 55$) of M-13-WT (fd virus).[32] We discuss this result briefly.

At first, a rough but intuitive estimation is made. It is reported that the initial decay rates $2\bar{\Gamma}_{20°C}$ of the homodyne correlation functions at $K = 1.22 \times 10^5$ cm^{-1} were 890 and 490 s^{-1} for dilute and semidilute ($cL^3 = 55$) solutions.[32] After T/η correction, we have $\bar{\Gamma}_{5°C} = 278$ s^{-1} and $\bar{\Gamma}_{5°C} = 153$ s^{-1} for dilute and semidilute solutions, respectively. At this K value, the contribution to $\bar{\Gamma}$ from bending motions is negligible (Figure 10a), so that we have the expression for $\bar{\Gamma}$ quoted in the Introduction. As mentioned before, we have $D_1 = 1.19 \times 10^{-8}$ cm^2/s, $D_3 = 1.87 \times 10^{-8}$ cm^2/s, $D_3 - D_1 = 0.68 \times 10^{-8}$ cm^2/s, and $\Theta = 13.1$ s^{-1} at 5 °C. Since $L = 0.895$ μm, we have $KL \simeq 11$ and hence $f_1(k) = 0.693$ and $f_2(k) = 0.0667$ (ref 16). Then we have $D_1K^2 + (L^2/12)\cdot\Theta f_1(k)K^2 + (D_3 - D_1)K^2f_2(k) = 177 + 90 + 7 = 274$ s^{-1}, which should be compared with the experimental value of $\bar{\Gamma}_{5°C} = 278$ s^{-1}. For a semidilute solution, we have an alternative[16]

$$\bar{\Gamma} = [1 - f_2(k)]\bar{D}_1K^2 + (L^2/12)\bar{\Theta}f_1(k)K^2 + D_3K^2f_2(k) \quad (72)$$

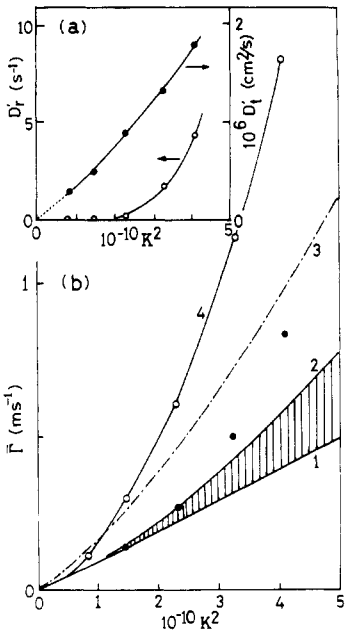

Figure 11. Experimental results for semidilute solutions of fd virus. (a) D_r' and D_t' vs. K^2 relationships.[32] (b) $\bar{\Gamma}$ vs. K^2 relationships. Curve 1: computed by use of eq 72 with $\bar{D}_1 = 0.72 \times 10^{-8}$ cm^2/s, $D_3 = 1.87 \times 10^{-8}$ cm^2/s, and $\bar{\Theta} = 5$ s^{-1} at 5 °C; curve 2: curve 1 *plus* contribution from the filament flexing (the shaded area shows the difference between solid curves for $\gamma L = 0.1$ and for rod in Figure 10a); curve 3: $\bar{\Gamma}$ for dilute solutions;[10] curve 4: computed by use of eq 74. (●) From two-exponential fit of computed correlation functions (for details, see text).

It is reported that $\bar{\Theta} \simeq 8$ s^{-1} at 20 °C and at $cL^3 = 55$ (ref 30 and 32) or $\bar{\Theta} \simeq 5$ s^{-1} at 5 °C. Then from eq 72 we have $\bar{D}_1 \simeq 0.72 \times 10^{-8}$ cm^2/s at 5 °C, which is about half the D_1 value!

In order to extend the above analysis to other K^2 values, we have to know the $\bar{\Gamma}$ values. Unfortunately, Maguire's paper did not give them, so we made the following trial. By putting $\langle q_m^2 \rangle = 0$ or $\exp[-\Phi(m,s,s',\xi,\xi,\tau)] = 1$ in eq 56, we have the Doi–Edwards expression ($\bar{D}_1 = 0$):

$$G^1(\tau) = \text{sech}\,(\bar{\mu}\bar{\Theta}\tau)\int_0^1 [j_0(k\xi)]^2 \exp[-\bar{\mu}\xi^2 \tanh\,(\bar{\mu}\bar{\Theta}\tau)]\,d\xi \quad (73)$$

After replacement of $\bar{\Theta} \to D_r'$, $D_3 \to D_t'$, and $\bar{\mu}^2 \to \gamma^2 = D_t'K^2/D_r'$, Maguire analyzed his data at $cL^3 = 55$ assuming both D_t' and D_r' as adjustable parameters. His result is quoted in Figure 11a. A method to obtain $\bar{\Gamma}$ values will be given as follows. From the relationship $\bar{\Gamma} = -(\partial/\partial\tau)\ln G^1(\tau)|_{\tau=0}$, we have from eq 73

$$\bar{\Gamma} = D_t'K^2\phi_2(k) \quad (\to D_t'K^2/3 \quad \text{as } k \to 0) \quad (74)$$

$$\phi_2(k) = \int_0^1 \xi^2[j_0(k\xi)]^2\,d\xi \Big/ \int_0^1 [j_0(k\xi)]^2\,d\xi \quad (75)$$

The initial decay rate of $G^1(\tau)$ in eq 73 is exclusively determined by the value of D_t' and the tail part of $G^1(\tau)$ by sech $(\gamma D_r'\tau) \propto \exp(-\gamma D_r'\tau)$. Unexpected results in Figure 11a came partly from these situations. We have immediately $\phi_2(0) = {}^1/_3$ and $\phi_2(\infty) = 0$. Numerical computation showed that $\phi_2(k)$ has the same values (to five digits) as $f_2(k)$ in eq 72. Then by using eq 74 and the tabulated values of $f_2(k)$ in ref 16, we could estimate the $\bar{\Gamma}$ values from the D_t' values in Figure 11a. Unfortunately, however, eq 74 gives $\bar{\Gamma}$ values that are much too large. For example, at $K = 1.22 \times 10^5$ cm^{-1}, Maguire gave $D_t' = 49.0 \times 10^{-8}$ cm^2/s at 20 °C (ref 32) or $D_t' = 30.6 \times 10^{-8}$ cm^2/s at 5 °C. Then eq 74 gives $\bar{\Gamma}_{5°C} = 304$ s^{-1}, which is just twice larger than $\bar{\Gamma}_{5°C} = 153$ s^{-1} from the experimental value. Except

for the $\bar{\Gamma}$ value at the lowest K^2, eq 74 gives $\bar{\Gamma}$ values (curve 4 in Figure 11b) which are larger than those for dilute solutions (curve 3 in Figure 11b). To see this inadequate situation, we computed $G^1(\tau)$ at $K = 1.22 \times 10^5$ cm^{-1} by use of eq 73 with Maguire's values of $D_t' = 30.6 \times 10^{-8}$ cm^2/s and $D_r' = 0.00375$ s^{-1} at 5 °C and evaluated the slope $\bar{\Gamma}_t$ defined by $\bar{\Gamma}_t = [\ln G^1(0) - \ln G^1(t)]/t$. The $\bar{\Gamma}_t$ values were 300 s^{-1} at $t = 20$ μs, 268 s^{-1} at $t = 200$ μs, and 159 s^{-1} at t = 2 ms. Although overall fitting was fairly good between experimental and computed (reconstructed) correlation functions, this result indicated that the computed correlation function had a very rapid component with a small amplitude, which decayed within $t = 200$ μs, an order of the channel width t_c inferred from Figure 2 in ref 32. Then we prepared $G^1(mt_c)$ ($m = 1, 2, ..., 64$) and analyzed it by a cumulant expansion and a two-exponential fitting. Because of a long tail in the correlation functions, a low-order cumulant expansion did not give a good fitting. Since we need only the initial decay rate of $G^1(mt_c)$, a cumulant analysis by use of a part of $G^1(mt_c)$ may be possible. But there is arbitrariness in termination at $m = M$ (<64). Instead, we computed $\bar{\Gamma} = (A_1\Gamma_1 + A_2\Gamma_2)/(A_1 + A_2)$ from a two-exponential least-squares analysis. The result is shown in Figure 11b (●). Curve 1 in Figure 11b represents eq 72 with $D_3 = 1.87 \times 10^{-8}$ cm^2/s, $\bar{\Theta} = 5$ s^{-1}, and $\bar{D}_1 = 0.72 \times 10^{-8}$ cm^2/s (the above estimated value at $K = 1.22 \times 10^5$ cm^{-1}). The shaded area shows the difference between solid curves for $\gamma L = 0.1$ and for rod in Figure 10a. Thus, curve 2 in Figure 11b approximately gives $\bar{\Gamma}$ for fd virus in semidilute solution at $cL^3 = 55$ when $\bar{D}_1$ is assumed to be independent of K. The large deviation of the estimated $\bar{\Gamma}$ at $K^2 \simeq 4 \times 10^{10}$ cm^{-2} from curve 2 could be reduced if the $\bar{D}_1$ value were raised. For $\bar{D}_1 = D_1$, this deviation becomes negligibly small. Although the estimated $\bar{\Gamma}$ values ((●) in Figure 11b) might be approximate because of very indirect deduction of them, the above discussion strongly suggests that the $\bar{D}_1$ value at large K^2 is close to D_1 and that the effect of the filament flexing is indispensable for the interpretation of the data for fd virus. In addition to these, the large n (l) terms of rotation (small angle-step rotations) also contribute to $\bar{\Gamma}$ at large K^2, resulting in a little increase in the $\bar{\Theta}$ value. At very larger KL values, $\bar{\Gamma}$ for a long and semiflexible filament in semidilute solution may behave like that for dilute solution.

6. Concluding Remarks

Recently, our theory for a dilute solution of a rigid rod was critically examined in an experimental study of monodisperse samples of tobacco mosaic virus.[17] Theoretical predictions were confirmed experimentally not only for the first cumulant but also for the whole decay profile of $G^1(\tau)$. Because of the limited amount of experimental data now available in the literature, the theory presented here has not yet been critically examined. Both for dilute and semidilute solutions of long and semiflexible filaments, it is important to directly compare our model with experimental data not only for the $\bar{\Gamma}$ values but also for the decay profiles of $G^1(\tau)$. At present, however, we can suggest that the experimental data for fd virus both in dilute and in semidilute solutions could not be explained without considering the effect of the filament flexing on both $\bar{\Gamma}$ and the decay profile of $G^1(\tau)$. Our finding of $\bar{D}_1 \simeq D_1/2$ at $K = 1.22 \times 10^5$ cm^{-1} and at $cL^3 = 55$ might be interesting, because this suggests the importance of the K dependence of $\bar{D}_1$ in polarized light scattering of a long (and semiflexible) rod in semidilute solution. A further study will be presented in the near future with our own experimental results.[34]

References and Notes

(1) Fujime, S. *J. Phys. Soc. Jpn.* **1970**, *29*, 751.
(2) Fujime, S.; Ishiwata, S. *J. Mol. Biol.* **1971**, *62*, 251.
(3) Ishiwata, S.; Fujime, S. *J. Mol. Biol.* **1972**, *68*, 511.
(4) Carlson, F. D.; Fraser, A. B. *J. Mol. Biol.* **1974**, *89*, 273.
(5) Fraser, A. B.; Eisenberg, E.; Kielley, W. W.; Carlson, F. D. *Biochemistry* **1975**, *14*, 2207.
(6) Maeda, T.; Fujime, S. *J. Phys. Soc. Jpn.* **1977**, *42*, 1983.
(7) Hochberg, A.; Low, W.; Tirosh, R.; Borejdo, J.; Oplatka, A. *Biochim. Biophys. Acta* **1977**, *460*, 308.
(8) Fujime, S.; Maruyama, M.; Asakura, S. *J. Mol. Biol.* **1972**, *68*, 347.
(9) Loh, E.; Ralston, E.; Schumaker, V. N. *Biopolymers* **1979**, *18*, 2549.
(10) Newman, J.; Carlson, F. D. *Biophys. J.* **1980**, *29*, 37.
(11) Gethner, J. S.; Gaskin, F. *Biophys. J.* **1978**, *24*, 505.
(12) Kubota, K.; Chu, B.; Fan, S.-F.; Dewey, M. M.; Brink, P.; Colflesh, D. E. *J. Mol. Biol.* **1983**, *166*, 329.
(13) Maeda, H.; Saito, N. *J. Phys. Soc. Jpn.* **1969**, *27*, 984.
(14) Schaefer, D. W.; Benedek, G. B.; Schofield, P.; Bradford, E. *J. Chem. Phys.* **1971**, *55*, 3884.
(15) Wilcoxon, J.; Schurr, J. M. *Biopolymers* **1983**, *22*, 849.
(16) Maeda, T.; Fujime, S. *Macromolecules* **1984**, *17*, 1157, where D_3 in eq 38a and $(2n - 5)$ in eq B2 should read $D_3/3$ and $(2n + 5)$, respectively.
(17) Kubota, K.; Urabe, H.; Tominaga, Y.; Fujime, S. *Macromolecules* **1984**, *17*, 2096.
(18) Doi, M.; Edwards, S. F. *J. Chem. Soc., Faraday Trans. 2* **1978**, *74*, 560.
(19) Maeda, T.; Fujime, S. *Macromolecules* **1981**, *14*, 809.
(20) Fujime, S.; Maeda, T.; Ishiwata, S. "Biomedical Applications of Laser Light Scattering"; Sattelle, D. S., et al., Eds.; Elsevier Biomedical Press: Amsterdam, 1982; p. 251.
(21) Although evident from the definition of vectors $\mathbf{A}^e$ and $\mathbf{A}^o$, a remark is given for subscripts specifying elements of various vectors and matrices. For even integers m and n, A_m and B_{mn} should read the $(m/2)$th element of a vector $\mathbf{A}$ and the $(n/2)$th element of the $(m/2)$th line of a matrix $\mathbf{B}$, respectively, where the "zeroth" element or line is included. For odd integers m and n, on the other hand, they should read the $[(m + 1)/2]$th element of the vector $\mathbf{A}$ and the $[(n + 1)/2]$th element of the $[(m + 1)/2]$th line of the matrix $\mathbf{B}$, respectively.
(22) Berne, B. J.; Pecora, R. "Dynamic Light Scattering"; Wiley: New York, London, Sydney, and Toronto, 1976.
(23) Fujime, S.; Kubota, K. *Macromolecules* **1984**, *17*, 441.
(24) Doi, M. *J. Phys. (Paris)* **1975**, *36*, 607.
(25) Mori, Y.; Ookubo, N.; Hayakawa, R.; Wada, Y. *J. Polym. Sci., Polym. Phys. Ed.* **1982**, *20*, 2111.
(26) Fujime, S. *J. Phys. Soc. Jpn.* **1971**, *31*, 1805.
(27) According to Harris and Hearst (Harris, R. A.; Hearst, J. E. *J. Chem. Phys.* **1966**, *44*, 2595), the flexural rigidity ϵ and the inverse of the statistical length γ are related by $\epsilon = 3k_BT/(4\gamma)$. Since we consider a slightly bendable rod, we assume $\tilde{q}(m,t)$ to be two-dimensional (see eq 14). For this reason, we take $2k_BT$ instead of $3k_BT$, i.e., $\epsilon = k_BT/(2\gamma)$.
(28) Takahashi, H.; Mori, M. *Publ. Res. Inst. Math. Sci. (Kyoto Univ.)* **1974**, *9*, 721.
(29) Genz, A. C.; Malik, A. A. *J. Comp. Appl. Math.* **1980**, *6*, 295.
(30) Maguire, J. F.; McTague, J. P.; Rondelez, F. *Phys. Rev. Lett.* **1980**, *45*, 1891; **1981**, *47*, 148.
(31) Zero, K. M.; Pecora, R. *Macromolecules* **1982**, *15*, 87.
(32) Maguire, J. F. *J. Chem. Soc., Faraday Trans. 2* **1981**, *77*, 513.
(33) Newman, J.; Swinney, H. L. Day, L. A. *J. Mol. Biol.* **1977**, *116*, 593.
(34) A theoretical modeling on the friction constant ζ will be found in: Fujime, S.; Maeda, T. *Macromolecules*, in press.